https://doi.org/10.1016/j.snb.2017.08.108

Tunability of Pd-nanogapped H2 sensors made on SiO2-coated Si micropillar arrays

Meng Zhao [a] , Man Hon Wong[b] , Chung Wo Ong[b] *, Ngai Hang Ng [b] and Hau Chung Man[c]

a Jiangsu Key Laboratory of Micro and Nano Heat Fluid Flow Technology and Energy Application, School of Mathematics and Physics, Suzhou University of Science and Technology, Suzhou 215009, P.R. China

b Department of Applied Physics and Materials Research Center, The Hong Kong Polytechnic University, Hung Hom, Kowloon, Hong Kong, P.R. China

c Department of Industrial and Systems Engineering, The Hong Kong Polytechnic University, Hung Hom, Kowloon, Hong Kong, People Republic of China

* Author to whom correspondence should be addressed. E-mail: c.w.ong@polyu.edu.hk; Tel: (852) 2766 5689; Fax: (852) 2333 7629

ABSTRACT

A micro-nano hybrid technique is implemented to produce Pd-nanogapped gas sensors with tunable H2 sensing properties. A sensor is made of a Pd film deposited on a SiO2-coated Si micropillar array. Through adjusting the structural parameters, nanogaps of tunable size and distribution are introduced into the Pd film. The electrical connectivity and the H2 sensing properties, including the dynamic range of detection, the shape of sensor response and mode of operation etc. are all adjustable. The method is scalable and compatible with Si-based processes. The design is also extendable for making multi-sensor arrays. The physical mechanisms involved in controlling the sensor properties are proposed and discussed.

Keywords: Pd nanogap; hydrogen sensor; tunable performance; Si micropillar; micro-nano hybrid technique

1. Introduction

Metal palladium (Pd) and many Pd-based alloys exhibit intriguing hydrogen (H2)- induced-volume-expansion effect (HIVE) [1-7]. This effect is potentially useful in H2 sensing application. One attractive approach is to introduce nanogaps into one of this group of materials. The nanogaps are narrowed or closed when exposed to H2. The resistance of the material is changed to reflect the variation of H2 concentration in the environment [2,8-10]. To date, bulk in the form of assembles of nanoparticles or

nanowires were widely used in the studies on this topic [11-15]. The spaces between the particulates are varied in H2 and responsible for the resistive change [1,16-19]. Thin film specimens were also made, in which nanocracks can be created by internal stresses generated by repeatedly exposing to H2 [20-23]. A common problem is that the distribution and shape of the nanogaps are difficult to control, such that the gas sensing properties are hardly reproducible in production. Even worst, nanocracks in the materials may deform when working in cyclic mode, causing the sensor performance to drift with time [21-24]. Co-workers are motivated to search for solution to improve the controllability and stability of gas sensing properties of nanogapped Pd-based sensors [2]. In this paper, we report the result of a method combining micromachining techniques and physical vapor deposition (PVD) deposition to fabricate nanogapped H2 hydrogen sensors, where the shape and distribution of the nanogaps are supposed to be controllable. Improved reproducibility and tunability of the gas sensing properties of the device are expected to be achieved. This approach is referred to as the "micro-nano hybrid" method in this article.

2. Review of HIVE effect and model

The resistance of the Pd-based sensing element in a sensor is affected by two mechanisms all related to the variation of H2 concentration. Mechanism I is associated with a metal-to-hydride transition which conducts in two stages. When H atoms are first dissolved interstitially in the Pd lattice, a face-center-cubic α-phase PdHx is formed. When the value of x exceeds 0.015, a β-phase emerges to coexist with the α- phase. Complete transition to β-phase occurs at x = 0.607 [5,25,26]. Meanwhile, the lattice constant increases from 0.3889–03890 nm of Pd to 0.3893–0.3895 nm of the α-phase (volume expansion ~0.347%), and then increases more significantly to 0.4013–0.4025 nm of the β- phase (volume expansion ~10%) [3,5]. The electrical resistivity increases coherently by ~5% and 80% from that of metal Pd [3]. For a nanogapped Pd-based material, an additional Mechanism II originating from the HIVE effect takes place. It can affect the nanogap size and hence the electrical connectivity of material. The resistance is changed accordingly. The change is much sharper and significant than that of Mechanism I, but the sign of the response is opposite. These two mechanisms contribute differently to the resistance change of a nanogapped Pd-based material. Under Mechanism I, the material is hydrogenated to exhibit a continuous and mild increase of the resistance over a broad range of H2 concentration. The change of the nanogap size is negligible such that Mechanism II is not effective. In moderate H2 concentration range, Mechanism II starts to become important. It initiates a sharp and fast resistance drop, and dominates the resistance change. The condition at which the two 5 mechanisms

are compensated to give a null resistance change is identified to be point of crossover. The idea of using the proposed micro-nano hybrid approach for making nanogapped H2 sensor is presented in Fig. 1a. A Pd film is deposited on an array of vertically aligned silicon (Si) micropillars If the fabrication techniques are properly selected, the shape and distribution of the micropillars and the separation of the micropillars, and the thickness of the metal film are accurately controlled to make the Pd film to contain nanogaps of desired dimension and distribution. The initial electrical connectivity of the Pd film is achieved, which is altered to exhibit some specific resistive response in H2. The actual H2 concentration dependence of the resistive response is expected to be tailorable by modulating the sensor's design. Three representative sensor designs, Configuration I, II and III as depicted schematically in Fig. 1b-d, are employed in this study. The targeted H2 concentration dependences of sensor response S (or responding curve) of the three designs are also depicted (on the right side), where $S \equiv (Ro-RH2)/RH2$, with Ro and RH2 to be the resistance of the sensor layer measured at one atmospheric pressure of air and a specific H2 concentration balanced in Ar, respectively. For Configuration I, the nanogaps in the Pd layer are narrow. The purpose is to allow Mechanism II to affect the resistance more effectively at lower H2 concentration. With increasing H2 concentration, RH2 first rises from Ro mildly and then drops sharply to below Ro when Mechanism II starts to dominate the trend. The value of S derived from the resistance change is small and negative ($Ro < RH2$) at first. It then rises to pass the crossover point at $S = 0$, and finally rises to approach a large and positive value ($Ro > RH2$) by exhibiting a slim 6 sigmoidal responding curve (Fig. 1b). The transition mainly occurs in a narrow dynamic range of H2 concentration. For Configuration II, a gold/chromium (Au/Cr) buffer layer is added between the Pd layer and the SiO2/Si micropillars. This metal layer provides a parallel conduction path along the planar direction of the Pd film. As a result, the resistance of the bilayer is low and insensitive to hydrogenation of the Pd layer. In other words, the influence of Mechanism I is suppressed. Until the H2 concentration is high enough for Mechanism II to take place, the nanogaps start to be narrowed. The sensor response S of this sample is thereby always positive ($S > 0$). The response curve of such a sensor configuration is in a sigmoidal shape covering a broad dynamic detection range of H2 concentration and does not contain a crossover point (Fig. 1c). For Configuration III, the nanogaps in the Pd layer are broader than those of the above two configurations. The Pd layer has a very poor initial electrical connectivity. It remains at a high resistance state at low H2 concentration where Mechanism I is not effective. Until H2 concentration reaches a threshold, nanogaps are narrowed or closed within a very narrow dynamic range of H2 concentration. Mechanism II takes place to result in a sharp and strong resistance drop. The response curve is expected to exhibit a step-function shape as depicted in Fig. 1d.

3. Experimental methods

We employed micromachining techniques to produce the micropillar array for utilizing their flexibility, reproducibility and accuracy in determining the pattern. We also used magnetron sputtering to deposit the Pd film for utilizing is accuracy in controlling the film thickness, for example by means of a quartz thickness monitor. The fabrication process for fabricating a sample device was presented in the flow chart as shown in Figure S1. Step 1: A 1-μm silicon dioxide (SiO2) layer was grown on a 4-inch n-type Si wafer by wet thermal oxidation in an ASM A400 oxidation furnace at 1100oC for 200 min. They plays the role of the mask for a deep etching process. Step 2: Photolithography was performed to produce a pattern on a layer of photoresist (AZ703). Step 3: The photoresist pattern was transferred to the thermal SiO2 layer by applying reactive ion etching with an STS Multiplex Advanced Oxide Ether system. The settings of the process were listed in Table S1. Step 4: The residual photoresist of step 3 was stripped off by applying reaction ion etching in a PS210 microwave plasma system. Step 5: A template consisting of high-aspect-ratio Si micropillars was fabricated using an STS Multiplex Advanced Silicon Etcher. The parameters used in the process were tabulated in Table S2. Step 6: A second SiO2 layer was then sputtered onto the top of the Si micropillar template to narrow down the width of the inter-pillar separations. Step 7: Au/Cr electrodes were added for electrical measurements using a deposition-photolithography-etching process. Step 8: A top Pd layer was sputtered onto specified locations on the Si wafer using a stainless steel shadow mask. [Meng: Is there a need to add a Step for adding a Au/Cr buffer layer? It could be written as : “For fabricating a sample 8 device of Configuration II, a step is added to sputter an Au/Cr buffer layer with a thickness of xxx nm on the tips of the SiO2 micropillars.”] Resistive hydrogen sensing responses of Pd nanogap arrays were measured using a homemade system [27]. A sample was placed on a stainless steel holder equipped with a heater, a thermocouple and Au-plated test pins. The sample holder was mounted inside a stainless steel measurement chamber for performing the tests. A standard test cycle was performed by filling in the chamber with synthetic air and hydrogen balanced in argon respectively, whereas the chamber was first evacuated with a rotary pump before changing a gas. The resistance of the sample was measured using a Keithley 617 electrometer. The data were automatically acquired with a computer.

4. Results and discussion

4.1 Configuration I: effect of using small nanogap size in Pd film

Figs. 2a-b are the top view image of the Si micropillar array used for making a sample device in Configuration I. The images were taken upon completion of deep etching of the Si substrate (Step 5). Each of the micropillars has a square cross section of an edge length = 5 μm. The height is ≈ 60 μm such that the aspect ratio is 12. The separation of adjacent micropillars is 2.2 μm. A second SiO2 layer was sputtered on top to further reduce the gap size. An example is shown in Fig. 2c, which is taken after sputtering a 2.5-μm SiO2 layer on top. The inset in Fig. 2a shows that the sputtered SiO2 exhibits a mushroom-cap shape. The term "SiO2-gap size", defined as the distance between two adjacent SiO2 caps, is important in specifying a sample 9 device. Its magnitude can be adjusted according to the total thickness of the SiO2 layer. Next, a Pd layer was sputtered on top. Its thickness is another parameter of the sensor. These two parameters jointly determine the final size of the nanogaps in the Pd layer deposited on top. Three samples of this configuration were fabricated. They are denoted as Sample A, B and C, respectively. They were made to have different SiO2-gap sizes equal to 100, 150 and 300 nm; and different thicknesses of the Pd layers equal to 400, 400 and 800 nm, respectively (Table 1). The purpose of using different combinations of the two parameters in this part of the study is to investigate whether the H2 concentration dependence of the resistive response of the sensors can be modulated by adjusting the nanogap size in the Pd layer. The measured sensor resistance, RH2, in the range of H2 concentration from 0.25 to 6% at 40oC are plotted in Fig. 3a-c. The derived sensor response, S, are plotted in Fig. 3 (d). From these results, one confirms that modulation of the hydrogen sensing properties is achievable. The key findings are summarized and discussed in the following.

(i) The resistances of the Pd films in the sensors measured at zero H2 concentration, Ro, are in common below 350 Ω. This indicates that the nanogaps in the Pd films are small. They exhibit some degree of electrical connectivity and are not completely insulating. For Sample A having the narrowest SiO2-gap of 100 nm and Pd film of a thickness of 400 nm, the resistance in air Ro = 86 Ω is the lowest. The nanogaps in the Pd layer are expected to be the narrowest. The electrical connectivity should be the strongest among the three samples. For Sample B having a wider SiO2-gap size of 150 nm and the same Pd film thickness, Ro = 338 Ω is the highest. This indicates that the nanogap size in the Pd film of 10 Sample B is the largest. The electrical connectivity of the Pd film is the poorest. For Sample C having the widest SiO2-gap = 300 nm, and a 2 times-thicker Pd film of 800 nm, an intermediate Ro of 152.7 Ω is detected. This suggests that increase in SiO2 gap size and Pd film thickness give

opposite effects on the nanogap size and electrical connectivity of the Pd film, and can mutually compensate with each other.

(ii) In low H2 concentration region, the resistance of each sensor, RH2, rises mildly with increasing H2 concentration under the influence of Mechanism I, until reaching a maximum limit. The sensor response S = (Ro-RH2)/Ro becomes more negative as seen in the negative linear region in Fig. 3d. Sample A and B have the same Pd film thickness of 400 nm. However, the Pd film of Sample A has a stronger electrical conductivity, such that Mechanism I is expected to be more effective. The value of S ends up with a more negative limit than that of Sample B. Furthermore, the Pd film of Sample C is two times thicker (800 nm). The influence of Mechanism I on the fractional change of the resistance is considered to be more significant, such that the value of S can reach the most negative limit among the three samples. [MENG: I revise your writing, but I am not sure whether the discussion on Sample C is correct.]

(iii) In higher H2 concentration region, under the influence of Mechanism II, the Pd film resistance drops from the maximum value. It returns to Ro and drops further. The change is steep. Correspondingly, S starts to increase towards the positive direction. It cuts the axis of S = 0 at the crossover point, and finally rises steeply to approach some positive limit (see the positive logarithmic region in Fig. 3d). Since Sample B has the poorest initial 11 electrical connectivity and a highest resistance Ro, the fractional change of the resistance, (Ro-RH2)/Ro, in this region is the largest, and hence it exhibits the highest positive limit of S. On the other hand, Sample A has the strongest electrical connectivity and a smallest Ro, such that it fractional change of resistance and hence the positive limit of S is the smallest among the three samples in this series.

(iv) The crossover point shifts towards the higher H2 concentration side in the sequence of Sample A to B to C. This feature is seen more clearly in Fig. 4a-c. The position of crossover is determined by the condition where Mechanism II becomes strong enough to narrow down the nanogap size significantly, so that it is also a function of the structural parameters of the Pd layer. In particular, though Sample C is regarded to have a medium electrical connectivity, its Pd layer is much thicker than those of other two, and hence it needs a higher H2 concentration for the effect of Mechanism II to become prominent. The crossover point is thus at a location of a higher H2 concentration.

(v) The responding curves of the three samples of this Configuration I commonly exhibit a narrow asymmetric sigmoidal shape, with the transition accomplished within in a very narrow width of 1% H2 concentration. This feature agrees quite well with the expected one as proposed in model described in Section 3 and sketched in Fig. 1(b) [1,2]. [Please check whether these references should appear here]

These results confirm the success in fine tuning the sensor properties with Configuration I by adjusting the SiO2-gap size and Pd film thickness. The response curve can be manipulated in terms of adjusting the maximum and minimum S values, and the position of crossover. It 12 should be noted that some other factors like temperature could also transition range of the response curve. Some reports state that the α-to-β phase transition occurs at 1–2% of H2 at 20oC, and shits to 3–5% H2 at ~50oC [3,4,28]. The degree of crystallization [5,29] and the presence of stresses at the Pd-micropillar interface [30,31] may also have influences on the result. [Meng: why these comments are relevant?]

4.2 Configuration II: effect of adding a metal buffer layer between SiO2 and Pd layers

A sample D of Configuration II was fabricated. It has a 100-nm SiO2-gap and a 400-nm thick Pd layer, and is made to have an additional 50-nm Au/5-nm Cr buffer layer inserted between the micropillars and the Pd layer. This metal buffer layer provides an additional coplanar conduction path in parallel to the Pd layer. RH2 of the bilayer remains low and becomes insensitive to the hydridation of the Pd film. In other words, Mechanism I is deactivated. Mechanism II is the sole effect affecting the change of RH2. The sensor response S derived from RH2 is always positive. Without the contribution from Mechanism I, the response of RH2 is discernable in rather low H2 concentration range (Fig. 3e and the inset). Fig. 4d further shows that the dynamic detection range of H2 concentration covers a broad H2 concentration range from $\approx$ 20 ppm to 6 %. It is much broader than those of Sample A, B and C of Configuration I.

It should be noted that the lowest detectable limit of the sample is comparable to those of many other Pd-nanogapped H2 sensors reported in literatures [32-34]. We further point out that the addition of the Au/Cr buffer layer gives a low base resistance Ro of 35 Ω. This sacrifices 13 the sensor response to some extent. This problem could be alleviated by jacking up Ro either by enlarging the SiO2-gap size or reducing the thickness of the Pd layer, or both.

4.3 Configuration III: effect of using large nanogap size in Pd film

A Sample E of Configuration III was fabricated to have a wide SiO2-gap of 300 nm and a 400-nm Pd layer (Table 1). It is found to be insulating and have a very high Ro of 3.35×1011 Ω. The nanogaps in the Pd film are believed to be wide, such that the electrical connectivity of the Pd film is weak. The H2 dependence of RH2 of the sample is shown in Fig. 3f. RH2 is found to drop from the initial Ro to a moderate RH2 of 328 Ω, showing a huge sensor response S over 109 at a H2 concentration of 6% (Fig. 4e). This result is more than ten times higher than the record achieved by nanogapped Pd sensors so far [19]. In addition, the response time is ~ 1 s, indicating that it is a very fast switching process for the Pd to transform from a rather "fragmented" stage to become a continuous state at the moment when Mechanism II starts to take place. The response curve behaves as if a step function. A sensor of this type is particularly suitable to be used as a one-off disposable sensor capable of giving a large and fast response.

4.4 Repeatability tests

The response of the sample devices of Configuration I and II are found to be highly stable and repeatable in cyclic tests. As shown in Fig. 5, the resistance changes of Sample A and D associated with alternative exposures to 4% H2 and air are plotted. One sees that lower and 14 upper bounds of the resistance changes are basically unchanged for more than 30 cycles. We attribute this result to the flexural compliance of the high-aspect-ratio micropillars, which can bend to release part of the stresses due to the HIVE of the Pd layer in the lateral direction. The integrity of the Pd layer thus be better retained, and the cyclic stability of the sensing properties can be better ensured.

5. Conclusion

In conclusion, a micro-nano hybrid approach is implemented to fabricate nanogapped Pd based H2 sensors of improved sensing properties. Three configurations are tried out for developing sensors suiting the needs of different applications. Through adjusting the SiO2-gap size and the thickness of the top Pd layer, or by adding a metal buffer layer between the SiO2 and Pd layers, the dynamic detection range of H2 concentration, the magnitude and shape of the responding curve etc become tailorable. The sensor outputs becomes more tunable and predictable. The sensor response against H2 concentration can be in the form of a slim sigmoidal curve with a crossover point; or a continuously varying curve with positive sign over a broad dynamic detection range of H2 concentration; or a step-function curve with an extremely large sensor response at certain H2 concentration. The output signal is highly stable and can

be easily adapted to a microprocessor to give a derived output. The proposed process is scalable and compatible with Si-based microfabrication processes. A pilot experiment was done to confirm the feasibility of integrating several sensors on a chip. Result shows the feasibility of making a sensor array for improving selectivity.

Acknowledgements

The work described in this paper is substantially supported by Research Grants Council of the Hong Kong Administrative Region (Project No.: PolyU 5016/08P, account code: B-Q10N; Project No.: 5242/11E, account codes: B-Q26D); Innovative Technology Fund (Project No.: ITS/558/09, ZP2U, account code: K.11.27.ZP2U); Internal grants of The Hong Kong Polytechnic University (account codes : G-UA7P, G-YBB6, G-YBFU and G-YM42) and the NSF of China (51502186, 11574227, 11374225, 11304218, 11247023, 21407111).

References

[1] F. Favier, E.C. Walter, M.P. Zach, T. Benter, R.M. Penner, Hydrogen sensors and switches from electrodeposited palladium mesowire arrays, Science 293 (2001) 2227-2231.

[2] J. Lee, W. Shim, J.S. Noh, W. Lee, Design rules for nanogap-based hydrogen gas sensors, ChemPhysChem 13 (2012) 1395-1403.

[3] F.A. Lewis, The palladium hydrogen system, Academic press, London, 1967.

[4] F.D. Manchester, A. San-Martin, J.M. Pitre, The H-Pd (hydrogen-palladium) system, J. Phase Equilib. 15 (1994) 62-83.

[5] B.D. Adams, A. Chen, The role of palladium in a hydrogen economy, Mater. Today 14 (2011) 282-289.

[6] M. Zhao, M.H. Wong, C.W. Ong, Achievement of controlled resistive response of nanogapped palladium film to hydrogen, Appl. Phys. Lett. 107 (2015) 033108.

[7] J. Lee, W. Shim, E. Lee, J.S. Noh, W. Lee, Highly mobile palladium thin films on an elastomeric substrate: nanogap-based hydrogen gas sensors, Angew. Chem. Int. Edit. 50 (2011) 5301-5305.

[8] B. Jang, W. Kim, M.J. Song, W. Lee, Thermal stability of the sensing properties in H2 sensors composed of Pd nanogaps on an elastomeric substrate, Sens. Actuators B 240 (2017) 186-192.

[9] W. Kim, B. Jang, H.S. Lee, W. Lee, Reliability and selectivity of H2 sensors composed of Pd film nanogaps on an elastomeric substrate, Sens. Actuators B 224 (2016) 547-551.

[10] B. Jang, S. Cho, C. Park, H. Lee, M.J. Song, W. Lee, Palladium nanogap-based H2 sensors 17 on a patterned elastomeric substrate using nanoimprint lithography, Sens. Actuators B 221 (2015) 593-598.

[11] L.G. Villanueva, F. Fargier, T. Kiefer, M. Ramonda, J. Brugger, F. Favier, Highly ordered palladium nanodot patterns for full concentration range hydrogen sensing, Nanoscale 4 (2012) 1964-1967.
[12] J.S. Lee, S.G. Kim, S. Cho, J. Jang, Porous palladium coated conducting polymer nanoparticles for ultrasensitive hydrogen sensors, Nanoscale 7 (2015) 20665-20673.
[13] M. Moreno, F.J. Ibanez, J.B. Jasinski, F.P. Zamborini, Hydrogen reactivity of palladium nanoparticles coated with mixed monolayers of alkyl thiols and alkyl amines for sensing and catalysis applications, J. Am. Chem. Soc. 133 (2011) 4389-4397.
[14] J.L. Zou, K.S. Iyer, C.L. Raston, Hydrogen-induced reversible insulator-metal transition in a palladium nanosphere sensor, Small 6 (2010) 2358-2361.
[15] D. Gupta, D. Dutta, M. Kumar, P.B. Barman, C.K. Sarkar, S. Basu, S.K. Hazra, A low temperature hydrogen sensor based on palladium nanoparticles, Sens. Actuators B 196 (2014) 215-222.
[16] C. Fournier, K. Rajoua, M.L. Doublet, F. Favier, Palladium-silver mesowires for the extended detection of H2, ACS Appl. Mater. Interfaces 5 (2013) 310-318.
[17] F. Yang, D.K. Taggart, R.M. Penner, Fast, sensitive hydrogen gas detection using single palladium nanowires that resist fracture, Nano Lett. 9 (2009) 2177-2182.
[18] Y. Im, C. Lee, R.P. Vasquez, M.A. Bangar, N.V. Myung, E.J. Menke, R.M. Penner, M.H. Yun, Investigation of a single Pd nanowire for use as a hydrogen sensor, Small 2 (2006) 18 356-358.
[19] R. Dasari, F.P. Zamborini, Hydrogen switches and sensors fabricated by combining electropolymerization and Pd electrodeposition at microgap electrodes, J. Am. Chem. Soc. 130 (2008) 16138-16139.
[20] S. Wagner, M. Hamm, A. Pundt, Huge hydrogen-induced resistive switching in percolating palladium thin films, Scr. Mater. 69 (2013) 756-759. [21]O. Dankert, A. Pundt, Hydrogen-induced percolation in discontinuous films, Appl. Phys. Lett. 81 (2002) 1618-1620.
[22] T. Kiefer, L.G. Villanueva, F. Fargier, F. Favier, J. Brugger, The transition in hydrogen sensing behavior in noncontinuous palladium films, Appl. Phys. Lett. 97 (2010).
[23] C.W. Ong, Y.M. Tang, Sputtering pressure dependence of hydrogen-sensing effect of palladium films, J. Mater. Res. 24 (2009) 1919-1927.
[24] Y.M. Tang, C.W. Ong, Analysis and improvement of cyclic stability of H2 sensing properties of Pd/Mg-Ni films, Int. J. Hydrogen Energ. 36 (2011) 10188-10196.
[25] N.R. Fong, P. Berini, R.N. Tait, Hydrogen sensing with Pd-coated long-range surface plasmon membrane waveguides, Nanoscale 8 (2016) 4284-4290.

[26] A. Ollagniera, A. Fabre, T. Thundat, E. Finot, Activation process of reversible Pd thin film hydrogen sensors, Sens. Actuators B 186 (2013) 258-262.
[27] M. Zhao, J.X. Huang, M.H. Wong, Y.M. Tang, C.W. Ong, Versatile computer-controlled system for characterization of gas sensing materials, Rev. Sci. Instrum. 82 (2011) 105001.
[28] F. Yang, D.K. Taggart, R.M. Penner, Joule heating a palladium nanowire sensor for 19 accelerated response and recovery to hydrogen gas, Small 6 (2010) 1422-1429.
[29] R. Bardhan, L.O. Hedges, C.L. Pint, A. Javey, S. Whitelam, J.J. Urban, Uncovering the intrinsic size dependence of hydriding phase transformations in nanocrystals, Nat. Mater. 12 (2013) 905-912.
[30] R. Gremaud, M. Gonzalez-Silveira, Y. Pivak, S.d. Man, M. Slaman, H. Schreuders, B. Dam, R. Griessen, Hydrogenography of PdHx thin films: influence of H-induced stress relaxation processes, Acta Mater. 57 (2009) 1209-1219.
[31] S. Wagner, A. Pundt, Electrical resistivity and hydrogen solubility of PdHc thin films, Acta Mater. 58 (2010) 1387-1394.
[32] J.S. Noh, H. Kim, B.S. Kim, E. Lee, H.H. Cho, W. Lee, High-performance vertical hydrogen sensors using Pd-coated rough Si nanowires, J. Mater. Chem. 21 (2011) 15935- 15939.
[33] T. Xu, M.P. Zach, Z.L. Xiao, D. Rosenmann, U. Welp, W.K. Kwok, G.W. Crabtree, Self-assembled monolayer-enhanced hydrogen sensing with ultrathin palladium films, Appl. Phys. Lett. 86 (2005) 203104.
[34] H. Jung, B. Jang, W. Kim, J.-S. Noh, W. Lee, Ultra-sensitive, One-time use hydrogen sensors based on sub-10nm nanogaps on an elastomeric substrate, Sens. Actuators B 178 (2013) 689-693.

Figure captions:

Fig. 1. (a) General structural features of a Pd-nanogapped H2 sensor made on a SiO2/Si micropillar array. (b-d) Schematic sketches of Configuration I, II and III and respective expected responding curve against H2 concentration.

Fig. 2. (a) Top view of the micropillar array covered by a thermal SiO2 layer (inset: the side view of sputtered SiO2-coated micropillars). (b) Magnified top view of the micropillars with thermal SiO2. (c) Top view of the micropillars covered with sputtered SiO2 and reduced gap width. (d) Further reduction of gap size by adding a Pd layer.

Fig. 3. (a-c) Resistive responses of Sample A, B and C against 0.25%–6% H2 at 40 oC, (d) H2 dependence of the sensor responses of Samples A, B and C; and (e-f) Resistive responses of Sample D and E 0.25%–6% H2 at 40 oC. Insets magnify the plots in low H2 concentration region.

Fig. 4. H2 concentration dependences of the sensor responses of Sample A to E. The shaded areas indicate the main responding range of individual sensors.

Fig. 5. Cyclic resistive responses of (a) Sample A and (b) Sample D measured when exposing them to 4% H2/Ar and air alternatively at 40 oC.

Table 1. Sample codes and fabrication parameters of the sensor samples.

Configuration	**Sample code**	**SiO_2-gap (nm)**	**Au/Cr buffer (nm)**	**Pd thickness (nm)**	**R_o (Ω)**	**Crossover (% of H_2)**
	A	100	–	400	86	3
I	B	150	–	400	338	3.25
	C	300	–	800	153	4.25
II	D	100	50/5	400	35	nil
III	E	300	–	400	3.35×10^{11}	6 (on-off)

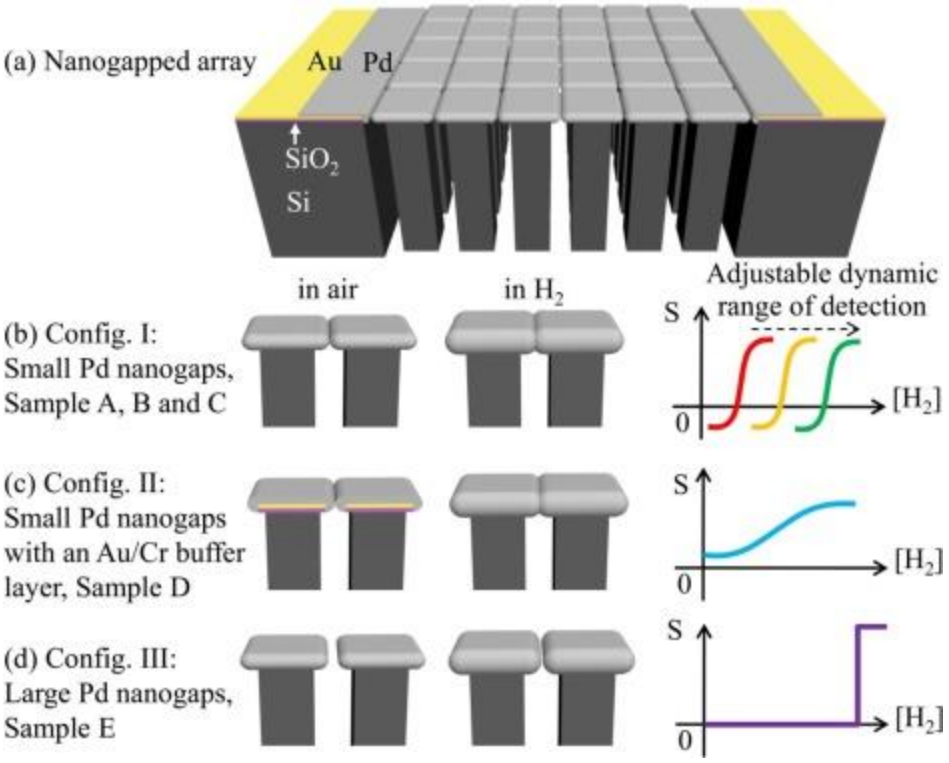

Fig 1. (a) General structural features of a Pd-nanogapped H_2 sensor made on a SiO_2/Si micropillar array. (b-d) Schematic sketches of Configuration I, II and III and respective expected responding curve against H_2 concentration.

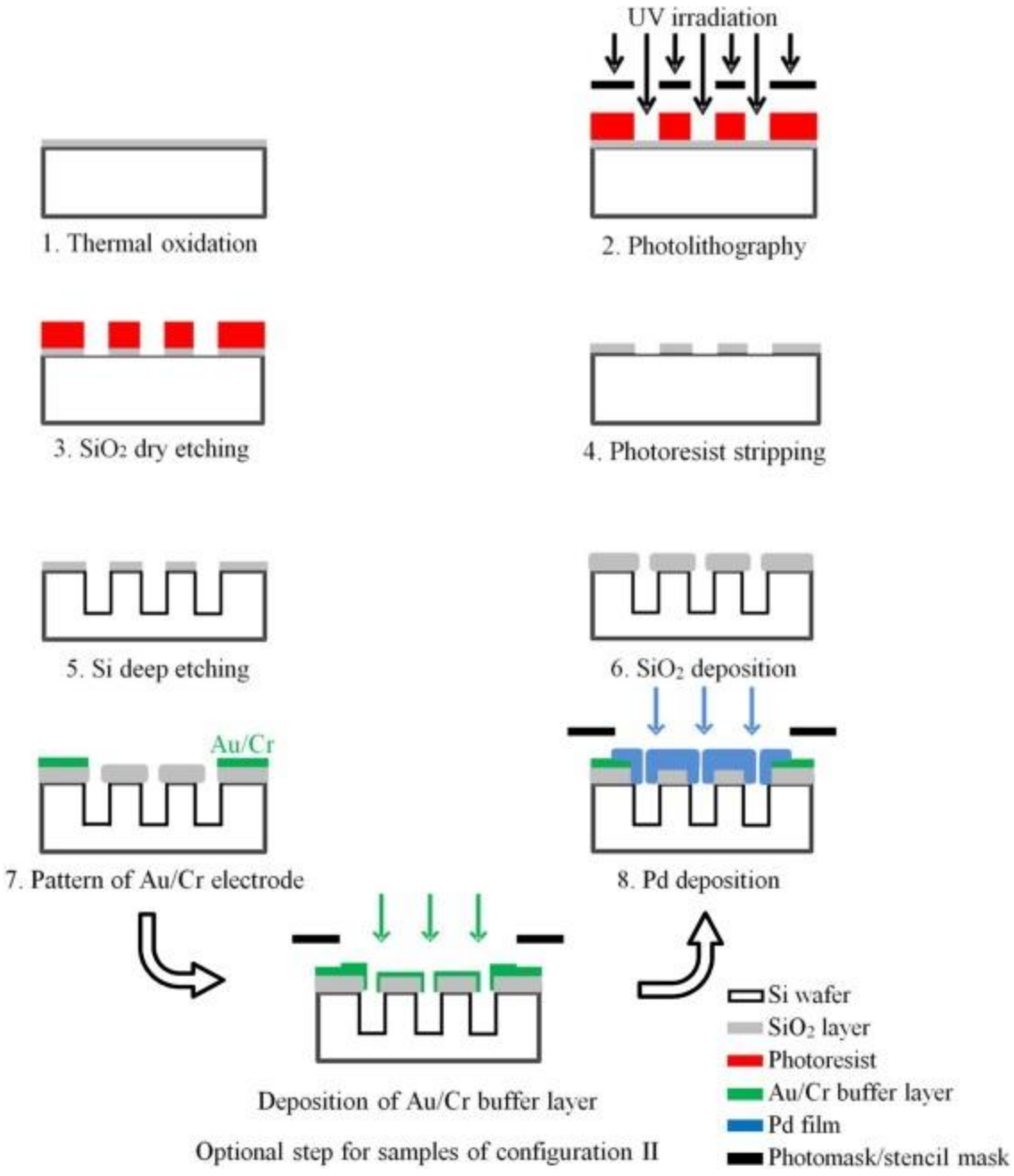

Fig. 2. (a) Top view of the micropillar array covered by a thermal SiO2 layer (inset: the side view of sputtered SiO2-coated micropillars). (b) Magnified top view of the micropillars with thermal SiO2. (c) Top view of the micropillars covered with sputtered SiO2 and reduced gap width. (d) Further reduction of gap size by adding a Pd layer.

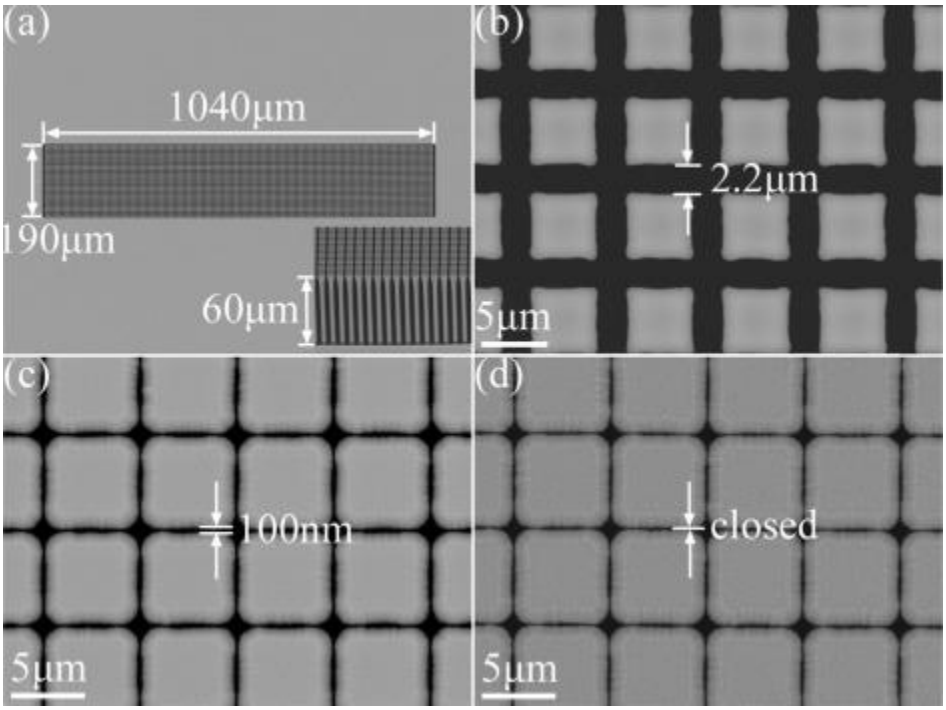

Fig. 3. (a-c) Resistive responses of Sample A, B and C against 0.25%–6% H2 at 40 oC, (d) H2 dependence of the sensor responses of Samples A, B and C

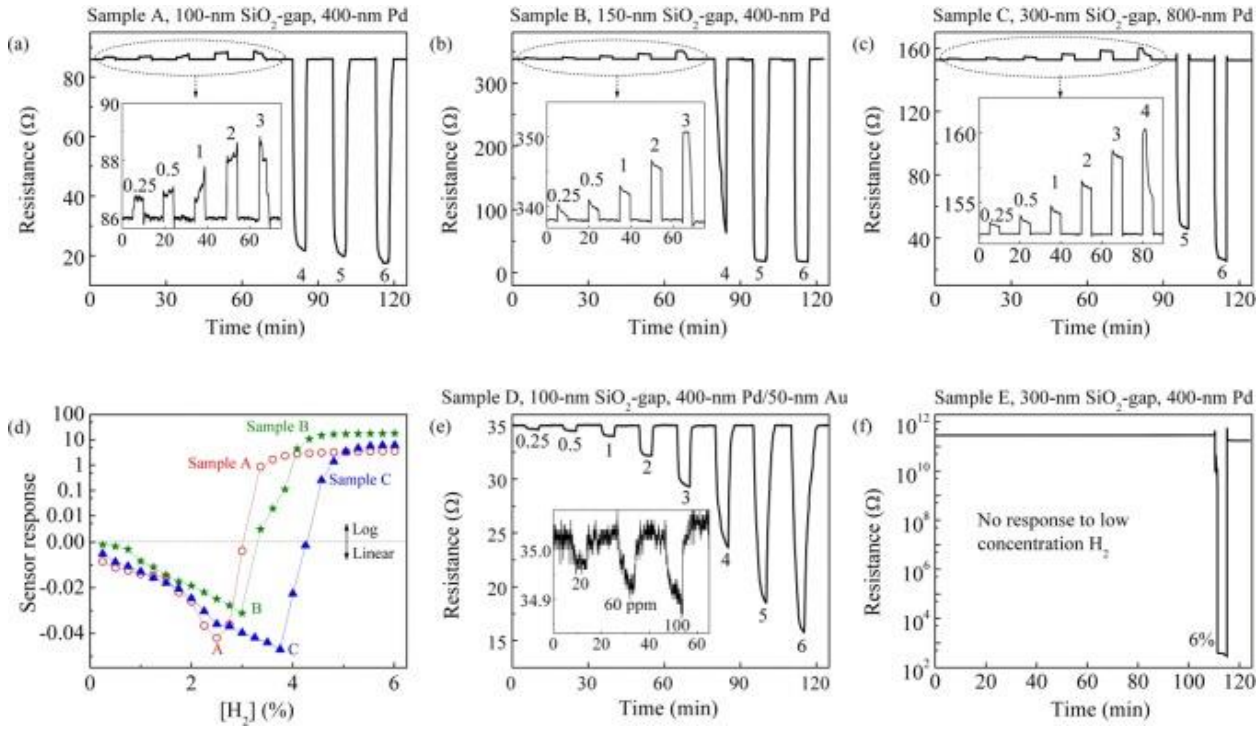

Fig. 4. (a–c) Resistive responses of Sample A, B and C against 0.25–6% H_2 at 40 °C, (d) H_2 dependence of the sensor responses of Samples A, B and C; and (e–f) Resistive responses of Sample D and E against 0.25–6% H_2 at 40 °C. Insets magnify the plots in low H_2 concentration region.

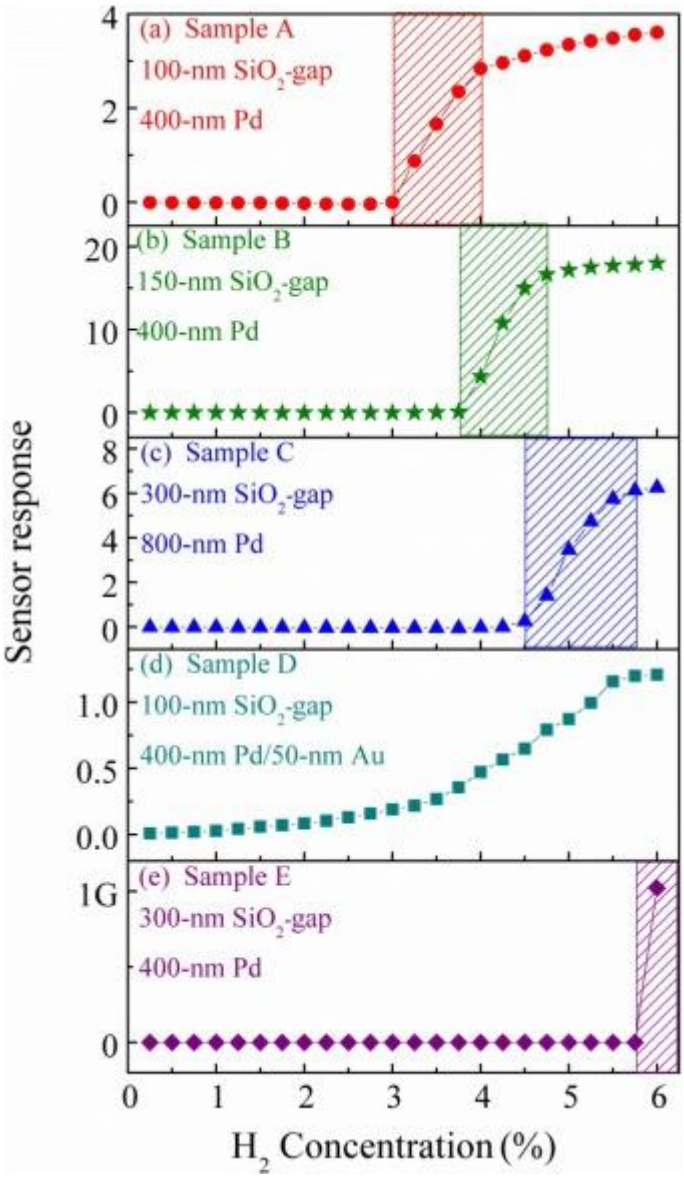

Fig. 5. H_2 concentration dependences of the sensor responses of Sample A to E. The shaded areas indicate the main responding range of individual sensors.

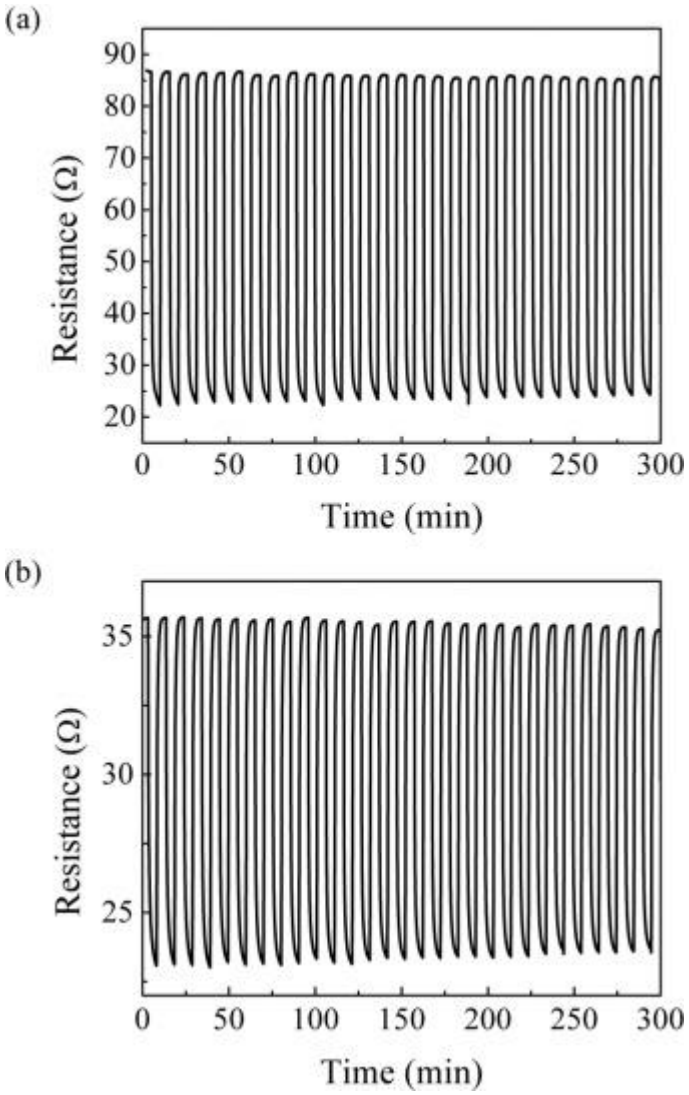

Fig. 6. Cyclic resistive responses of (a) Sample A and (b) Sample D measured when exposing them to 4% H_2 and air alternatively at 40 °C.

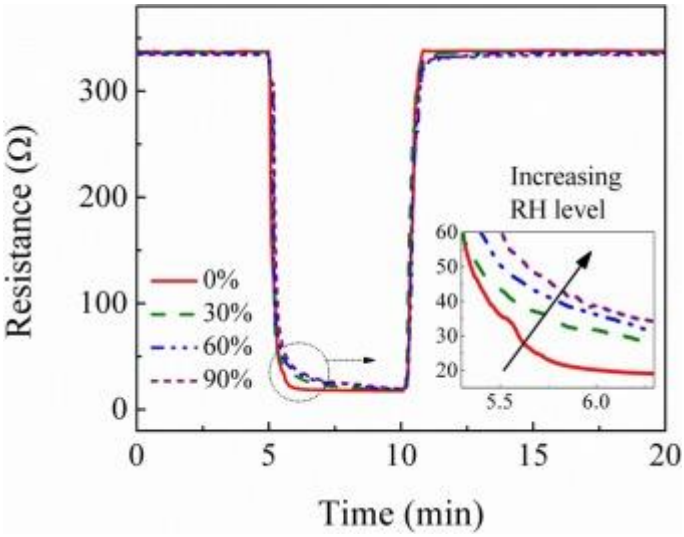

Fig. 7. Resistive responses of Sample B against 6% H_2 measured at 0%, 30%, 60% and 90% relative humidity. Data were recorded at 40 °C.